Inorg. Chem. **2008**, *47*, 4173−4184

$F_5SN(H)Xe^+$; a Rare Example of Xenon Bonded to sp^3-Hybridized Nitrogen; Synthesis and Structural Characterization of $[F_5SN(H)Xe][AsF_6]$

Gregory L. Smith, Hélène P. A. Mercier, and Gary J. Schrobilgen*

Contribution from the Department of Chemistry, McMaster University, Hamilton, Ontario L8S 4M1, Canada

Received October 14, 2007

The salt $[F_5SN(H)Xe][AsF_6]$ has been synthesized by the reaction of $[F_5SNH_3][AsF_6]$ with XeF_2 in anhydrous HF (aHF) and BrF_5 solvents and by solvolysis of $[F_3S{\equiv}NXeF][AsF_6]$ in aHF. Both $F_5SN(H)Xe^+$ and $F_5SNH_3^+$ have been characterized by ^{129}Xe, ^{19}F, and ^1H NMR spectroscopy in aHF (−20 °C) and BrF_5 (supercooled to −70 °C). The yellow $[F_5SN(H)Xe][AsF_6]$ salt was crystallized from aHF at −20 °C and characterized by Raman spectroscopy at −45 °C and by single-crystal X-ray diffraction at −173 °C. The Xe−N bond length (2.069(4) Å) of the $F_5SN(H)Xe^+$ cation is among the shortest Xe−N bonds presently known. The cation interacts with the AsF_6^- anion by means of a Xe---F−As bridge in which the Xe---F distance (2.634(3) Å) is significantly less than the sum of the Xe and F van der Waals radii (3.63 Å) and the AsF_6^- anion is significantly distorted from O_h symmetry. The ^{19}F and ^{129}Xe NMR spectra established that the $[F_5SN(H)Xe][AsF_6]$ ion pair is dissociated in aHF and BrF_5 solvents. The $F_5SN(H)Xe^+$ cation decomposes by HF solvolysis to $F_5SNH_3^+$ and XeF_2, followed by solvolysis of $F_5SNH_3^+$ to SF_6 and NH_4^+. A minor decomposition channel leads to small quantities of F_5SNF_2. The colorless salt, $[F_5SNH_3][AsF_6]$, was synthesized by the HF solvolysis of $F_3S{\equiv}NAsF_5$ and was crystallized from aHF at −35 °C. The salt was characterized by Raman spectroscopy at −160 °C, and its unit cell parameters were determined by low-temperature X-ray diffraction. Electronic structure calculations using MP2 and DFT methods were used to calculate the gas-phase geometries, charges, bond orders, and valencies as well as the vibrational frequencies of $F_5SNH_3^+$ and $F_5SN(H)Xe^+$ and to aid in the assignment of their experimental vibrational frequencies. In addition to $F_5TeN(H)Xe^+$, the $F_5SN(H)Xe^+$ cation provides the only other example of xenon bonded to an sp^3-hybridized nitrogen center that has been synthesized and structurally characterized. These cations represent the strongest Xe−N bonds that are presently known.

Introduction

Until recently, the only known Xe−N bonded compounds were those containing sp^2- or sp-hybridized nitrogen centers, namely, $FXeN(SO_2F)_2$,[1−3] $Xe[N(SO_2F)_2]_2$,[2,4] $F[XeN(SO_2F)_2]_2^+$,[2,4,5] $XeN(SO_2F)_2^+$,[5] $Xe[N(SO_2CF_3)_2]_2$,[6] and the XeF^+ adducts of HCN,[7,8] alkylnitriles,[7] pentafluorobenzenenitrile,[7] perfluoroalkylnitriles,[7,9] perfluoropyridines,[10] and *s*-trifluorotriazine.[9] Until the present work, the only example of a noble gas bonded to a formally sp^3-hybridized nitrogen atom was $[F_5TeN(H)Xe][AsF_6]$, which was recently reported from this laboratory.[11] The $F_5TeN(H)Xe^+$ cation represents the most covalent Xe−N bonded species reported to date and was synthesized by reaction of the XeF^+ cation with F_5TeNH_2 in anhydrous HF (aHF), and by reaction of $F_5TeNH_3^+$ and XeF_2 in aHF and BrF_5 solvents. Most recently, the synthesis and structural characterization of the

* Author to whom correspondence should be addressed. E-mail: schrobil@mcmaster.ca.

(1) LeBlond, R. D.; DesMarteau, D. D. *J. Chem. Soc., Chem. Commun.* **1974**, 555–556.
(2) DesMarteau, D. D.; LeBlond, R. D.; Hossain, S. F.; Nothe, D. *J. Am. Chem. Soc.* **1981**, *103*, 7734–7739.
(3) Sawyer, J. F.; Schrobilgen, G. J.; Sutherland, S. J. *Inorg. Chem.* **1982**, *21*, 4064–4072.
(4) Schumacher, G. A.; Schrobilgen, G. J. *Inorg. Chem.* **1983**, *22*, 2178–2183.
(5) Faggiani, R.; Kennepohl, D. K.; Lock, C. J. L.; Schrobilgen, G. J. *Inorg. Chem.* **1986**, *25*, 563–571.
(6) Foropoulos, J. J.; DesMarteau, D. D. *J. Am. Chem. Soc.* **1982**, *104*, 4260–4261.
(7) Emara, A. A. A.; Schrobilgen, G. J. *J. Chem. Soc., Chem. Commun.* **1987**, 1644–1646.
(8) Emara, A. A. A.; Schrobilgen, G. J. *Inorg. Chem.* **1992**, *31*, 1323–1332.
(9) Schrobilgen, G. J. *J. Chem. Soc., Chem. Commun.* **1988**, 1506–1508.
(10) Emara, A. A. A.; Schrobilgen, G. J. *J. Chem. Soc., Chem. Commun.* **1988**, 257–259.
(11) Fir, B. A.; Whalen, J. M.; Mercier, H. P. A.; Dixon, D. A.; Schrobilgen, G. J. *Inorg. Chem.* **2006**, *45*, 1978–1996.

10.1021/ic702039f CCC: $40.75 © 2008 American Chemical Society
Published on Web 04/12/2008

$F_3S{\equiv}NXeF^+$ cation, a rare example of a noble-gas compound in which the noble-gas atom is bonded to an inorganic sp-hybridized nitrogen center, was reported by the authors.[12] In the latter study, the previously demonstrated Lewis basicity of thiazyl trifluoride, $N{\equiv}SF_3$,[13] was exploited by reaction of the Lewis acidic XeF^+ cation,[14] as its AsF_6^- salt, with $N{\equiv}SF_3$ to form $[F_3S{\equiv}NXeF][AsF_6]$.[12]

In view of the solvolytic behavior of $N{\equiv}SF_3$ in aHF, which gives rise to F_5SNH_2[15] and to $[F_5SNH_3][AsF_6]$[16] in the superacidic medium AsF_5/aHF, and the basicity of F_5SNH_2, which forms the room-temperature stable Lewis acid–base adducts, $F_5SNH_2{\cdot}BF_3$ and $F_5SNH_2{\cdot}PF_5$,[17] two synthetic approaches to the formation of the $F_5SN(H)Xe^+$ cation were developed that are described in the present paper: (1) the reaction of $[F_5SNH_3][AsF_6]$ with XeF_2 in aHF and BrF_5 solvents and (2) the HF solvolysis of $[F_3S{\equiv}NXeF][AsF_6]$, providing avenues to the second example of xenon bound to a formally sp^3-hybridized nitrogen center.

Results and Discussion

Syntheses of $[F_5SNH_3][AsF_6]$ and $[F_5SN(H)Xe][AsF_6]$. The solvolytic reactions leading to the $F_5SNH_3^+$ and $F_5SN(H)Xe^+$ cations and their further solvolyses were monitored by ^1H, ^{19}F, and ^{129}Xe NMR spectroscopy in both aHF and BrF_5 solvents. The NMR parameters reported in this section (parameters obtained in BrF_5 are given in parentheses) are for previously known species and are not further discussed. Those of the title species are discussed in the NMR Spectroscopy section that follows.

(a) $[F_5SNH_3][AsF_6]$. The donor-acceptor adduct, $F_3S{\equiv}NAsF_5$, was prepared as previously described,[18] by reaction of $N{\equiv}SF_3$ with AsF_5 at −78 °C for ca. 1 h, forming a friable white solid. The ammonium salt, $[F_5SNH_3][AsF_6]$, was synthesized as previously described[16] by reaction of $F_3S{\equiv}NAsF_5$ with aHF at 0 °C for ca. 6 h (eq 1), forming colorless, featherlike crystals. In both instances, the products were characterized by Raman spectroscopy at −160 °C.

$$F_3S{\equiv}NAsF_5 + 3HF \xrightarrow[HF]{0\ ^\circ C} [F_5SNH_3][AsF_6] \qquad (1)$$

(b) $[F_5SN(H)Xe][AsF_6]$. The solvolysis of $[F_3S{\equiv}NXeF][AsF_6]$[12] in aHF over a period of ca. 4 h at −20 °C led to $[F_5SN(H)Xe][AsF_6]$ formation according to eq 2. The salt was obtained as transparent yellow plates and was characterized by Raman spectroscopy at −45 °C. The $F_5SN(H)Xe^+$ cation was also formed by reaction of $[F_5SNH_3][AsF_6]$ with XeF_2 in aHF and BrF_5 solvents (eq 3) at −30 °C for ca. 30 min and was characterized by ^{19}F NMR spectroscopy (at −20 °C and supercooled to −70 °C, respectively). In both synthetic approaches, $F_5SNH_3^+$ and $F_5SN(H)Xe^+$ were observed in equilibrium with XeF_2 and HF, so that eq 3 is best described as a solvent- and temperature-dependent equilibrium. In BrF_5 and aHF solutions below −20 °C, equilibrium 3 lies to the right, while in aHF above −20 °C, no $F_5SN(H)Xe^+$ is observed.

$$[F_3S{\equiv}NXeF][AsF_6] + HF \xrightarrow[HF]{-20\ ^\circ C} [F_5SN(H)Xe][AsF_6] \qquad (2)$$

$$[F_5SNH_3][AsF_6] + XeF_2 \underset{BrF_5}{\overset{HF\ or}{\rightleftharpoons}} [F_5SN(H)Xe][AsF_6] + 2HF \qquad (3)$$

(c) Decompositions of $[F_5SNH_3][AsF_6]$ and $[F_5SN(H)Xe][AsF_6]$ in aHF. The decompositions of $[F_5SNH_3][AsF_6]$ and $[F_5SN(H)Xe][AsF_6]$ in aHF at 0 °C were monitored by ^{19}F NMR spectroscopy. The $F_5SN(H)Xe^+$ cation underwent solvolysis in aHF to form $F_5SNH_3^+$ and XeF_2 [$\delta(^{19}F)$ = −194.5 (−185.0) ppm, $^1J(^{19}F{-}^{129}Xe)$ = 5652 (5611) Hz] according to the reverse of eq 3. The $F_5SNH_3^+$ cation underwent further solvolysis (eq 4) to form SF_6 [$\delta(^{19}F)$ = 54.1 (56.0) ppm, $^1J(^{19}F{-}^{33}S)$ = 251.9 Hz] and NH_4^+ [$\delta(^1H)$ = 5.54 ppm, $^1J(^1H{-}^{14}N)$ = 51 Hz]. Small amounts of F_5SNF_2 also formed in the course of $F_5SN(H)Xe^+$ decomposition. The $[F_5SNH_3^+]/[F_5SN(H)Xe^+]/[F_5SNF_2]/[SF_6]$ molar ratios at −20 °C in BrF_5 and aHF were 1.00:0.17:0.02:0.47 and 1.00:0.01:0.01:0.44, respectively.

$$[F_5SNH_3][AsF_6] + HF \xrightarrow[HF]{-20\ to\ 0\ ^\circ C} SF_6 + [NH_4][AsF_6] \qquad (4)$$

The formation of F_5SNF_2 likely results from a series of reactions (eqs 5−10) analogous to those leading to F_5TeNF_2, also a minor product in the decomposition of the $F_5TeN(H)Xe^+$ cation.[11] The decomposition of $F_5SN(H)Xe^+$ to form F_5SNF_2 is consistent with the nucleophilic fluorination of $F_5SN(H)Xe^+$ accompanied by the liberation of xenon gas and formation of the nitrenium ion, F_5SNF^+, as an intermediate (eq 5). Nucleophilic attack by the F^- ion leads to the known fluoramine, F_5SNHF, according to eq 6.[19] The enhanced fluoroacidity that results from fluorination of the nitrenium cation (eq 6) also results in the formation of the strong oxidant cations, XeF^+ and $Xe_2F_3^+$ (eqs 7 and 8), which may be expected to fluorinate F_5SNHF to $F_5SNHF_2^+$ (eq 9). The $F_5SNHF_2^+$ cation is expected to readily deprotonate (eq 10) by analogy with NF_3, which is too weakly basic to be protonated in the AsF_5/HF solution.[20] The NMR parameters determined for F_5SNF_2 in HF at −20 °C in this work [$\delta(^{19}F_{eq})$ = 31.5 ppm (doublet of triplets), $\delta(^{19}F_N)$ = 66.3 ppm (quintet), $^2J(^{19}F_{ax}{-}^{19}F_{eq})$ = 157.1 Hz and $^3J(^{19}F_N{-}^{19}F_{eq})$ = 13.8 Hz] are in good agreement with the previously reported parameters [$\delta(^{19}F_{ax})$ = 48.5 ppm (quintet),[21] $\delta(^{19}F_{eq})$ = 36.5 ppm (doublet of triplets),[21]

(12) Smith, G. L.; Mercier, H. P. A.; Schrobilgen, G. J. *Inorg. Chem.* **2007**, *46*, 1369–1378.
(13) Glemser, O.; Mews, R. *Angew. Chem., Int. Ed. Engl.* **1980**, *19*, 883–899.
(14) Schrobilgen, G. J. In *Synthetic Fluorine Chemistry*; Olah, G. A., Chambers, R. D., Prakash, G. K. S., Eds.; John Wiley & Sons: New York, 1992; pp 1–30.
(15) Clifford, A. F.; Duncan, L. C. *Inorg. Chem.* **1966**, *5*, 692–693.
(16) Meier, T.; Hoppenheit, R.; Mews, R. *Z. Anorg. Allg. Chem.* **1993**, *619*, 1241–1246.
(17) Clifford, A. F.; Zeilenga, G. R. *Inorg. Chem.* **1969**, *8*, 1789–1791.
(18) Glemser, O.; Koch, W. *An. Asoc. Quim. Argent.* **1971**, *59*, 143–148.
(19) DesMarteau, D. D.; Eysel, H. H.; Oberhammer, H.; Günther, H. *Inorg. Chem.* **1982**, *21*, 1607–1616.
(20) Christe, K. O. *Inorg. Chem.* **1975**, *14*, 2821–2824.
(21) Stump, E. C., Jr.; Padgett, C. D.; Brey, W. S., Jr. *Inorg. Chem.* **1963**, *2*, 648–649.

Table 1. NMR Chemical Shifts and Spin-Spin Coupling Constants for $[F_5SNH_3][AsF_6]$ and $[F_5SN(H)Xe][AsF_6]$[a]

species	chemical shifts, ppm			coupling constants, Hz
	$\delta(^{129}Xe)$	$\delta(^{19}F)$	$\delta(^{1}H)$	$^2J(^{19}F_{ax}-^{19}F_{eq})$
$F_5SNH_3^+$		50.1 (50.0), F_{ax} 71.7 (73.8), F_{eq}	8.92 (7.74)	152.6 (154.7)
$F_5SN(H)Xe^+$	−2897 (−2956)	59.0 (59.6), F_{ax} 71.3 (73.0), F_{eq}	(9.57)	152.9 (154.7)
AsF_6^-[b]		−69 (−64)		
SF_6[c]		54.1 (56.0)		
NH_4^+[d]			5.54	
XeF_2[e]		−194.5 (−185.0)		
HF		−197 (−192)	8.26 (7.39)	
BrF_5		(134.5), F_{eq} (272.0), F_{ax}		(76.3)

[a] The values in parentheses were measured in supercooled BrF_5 solvent at −70 °C; all other values were measured in aHF solvent at −20 °C. The axial and equatorial fluorines are denoted by F_{ax} and F_{eq}, respectively. The secondary isotope shifts arising from $^{34/32}S$ were measured in the ^{19}F NMR spectra of $F_5SNH_3^+$ and $F_5SN(H)Xe^+$ in aHF solvent: $^1\Delta^{19}F_{ax}(^{34/32}S) = -0.058$ and −0.060 ppm, and $^1\Delta^{19}F_{eq}(^{34/32}S) = -0.056$ and −0.056 ppm, respectively. [b] The ^{19}F resonance of the AsF_6^- anion was broad and saddle-shaped in aHF [$\Delta\nu_{1/2} = 2860$ (700) Hz] as a result of partial quadrupolar collapse of the 1:1:1:1 quartet arising from $^1J(^{75}As-^{19}F)$. [c] The secondary isotope effects of $^{34/32}S$ on ^{19}F, $^1\Delta^{19}F_{ax}(^{34/32}S) = -0.052$ ppm, and $^1J(^{19}F-^{33}S) = 251.9$ Hz were observed in aHF solvent at −20 °C. [d] $^1J(^1H-^{14}N) = 51$ Hz. [e] $^1J(^{19}F-^{129}Xe) = 5652$ (5611) Hz.

$\delta(^{19}F_N) = 66.3$ ppm (quintet),[21] $^2J(^{19}F_{ax}-^{19}F_{eq}) = 153.2$ Hz,[22] and $^3J(^{19}F_N-^{19}F_{eq}) = 19$ Hz[21]]. In the present study, the axial fluorine resonance was obscured by overlap with the axial fluorine resonance of $F_5SNH_3^+$ (49.9 ppm, aHF, −20 °C). The $^3J(^{19}F_N-^{19}F_{ax})$ coupling was not resolved in the present and prior studies, in accordance with the general inability to resolve three-bond couplings to the axial fluorine of the F_5Te moiety.[23] Similarly, the $^3J(^{19}F_N-^{19}F_{ax})$ coupling also was not resolved in F_5TeNF_2.[11]

$$F_5SN(H)Xe^+ \rightarrow [F_5SNH^+] + Xe \quad (5)$$

$$[F_5SNH^+] + 2HF/AsF_6^- \rightarrow F_5SNHF + H_2F^+/AsF_5 \quad (6)$$

$$AsF_5 + XeF_2 \rightleftharpoons [XeF][AsF_6] \quad (7)$$

$$[XeF][AsF_6] + XeF_2 \rightleftharpoons [Xe_2F_3][AsF_6] \quad (8)$$

$$F_5SNHF + XeF^+(Xe_2F_3^+) \rightarrow F_5SNHF_2^+ + Xe\ (Xe + XeF_2) \quad (9)$$

$$F_5SNHF_2 + HF \rightarrow F_5SNF_2 + H_2F^+ \quad (10)$$

NMR Spectroscopy. The ^1H, ^{19}F, and ^{129}Xe NMR parameters for $[F_5SNH_3][AsF_6]$ and $[F_5SN(H)Xe][AsF_6]$, recorded in aHF solvent at −20 °C or BrF_5 supercooled to −70 °C, are listed in Table 1 (NMR parameters obtained in BrF_5 are given in parentheses). The chemical shifts and coupling constants are in accord with those of other F_5S derivatives,[16,24] $F_5TeNH_3^+$,[11] and $F_5TeN(H)Xe^+$.[11]

(a) $[F_5SNH_3][AsF_6]$. The ^{19}F NMR spectrum of the $F_5SNH_3^+$ cation (Figure S1) is an AX_4 spin-coupling pattern, occurring at 71.7 (73.8) [doublet, F_{eq}] and 50.1 (50.0) [quintet, F_{ax}] ppm with $^2J(^{19}F_{ax}-^{19}F_{eq}) = 152.6$ (154.7) Hz, that arises from the pseudo-octahedral F_5SN group. These parameters are in good agreement with those previously reported for $F_5SNH_3^+$ in liquid SO_2: 76.37 and 52.43 ppm and 156.5 Hz (−40 °C), respectively.[16]

The ^1H NMR spectrum of $[F_5SNH_3][AsF_6]$ consists of a broad singlet at 8.92 (7.74) ppm [$\Delta\nu_{1/2} = 23.0$ (54.2) Hz]. This chemical shift is in agreement with that reported in liquid SO_2: 8.8 ppm (−40 °C).[16] The line broadening and absence of resolved couplings results from quadrupolar relaxation by the directly bonded ^{14}N atom ($I = 1$).

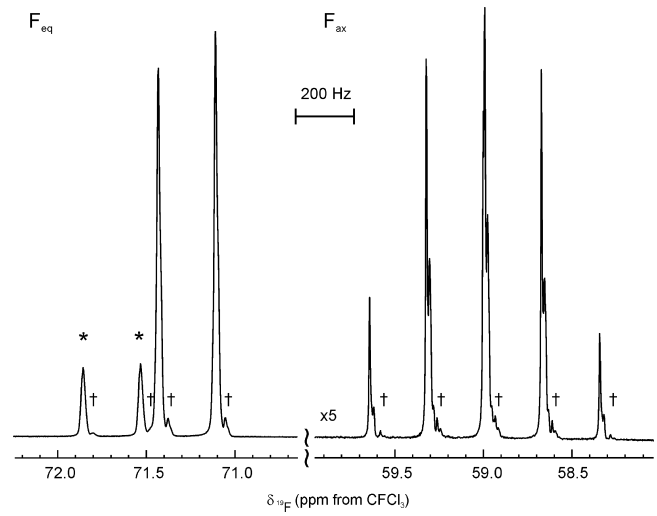

Figure 1. The ^{19}F NMR spectrum (470.592 MHz) of $F_5SN(H)Xe^+$ in HF solvent at –20 °C. Symbols denote the secondary isotope shifts, $^1\Delta^{19}F(^{34/32}S)$, on F_{eq} and F_{ax} (†), and F_{eq} of $F_5SNH_3^+$ (*).

(b) $[F_5SN(H)Xe][AsF_6]$. The NMR spectra are consistent with eqs 2 and 3 in which resonances arising from $F_5SNH_3^+$, SF_6, and NH_4^+ (vide supra) (eqs 3 and 4) were also observed.

The ^{19}F NMR spectrum of $F_5SN(H)Xe^+$ (Figure 1) consists of an AB_4 spin-coupling pattern at 71.3 (73.0) [doublet, F_{eq}] and 59.0 (59.6) [quintet, F_{ax}] ppm, with $^2J(^{19}F_{ax}-^{19}F_{eq}) = 152.9$ (154.7) Hz, that arises from the pseudo-octahedral F_5SN group. These parameters are very similar to those of $F_5SNH_3^+$ (vide supra), except for the equatorial fluorine chemical shift, which is significantly more deshielded in the xenon cation, a trend that was also observed for the $F_5TeN(H)Xe^+$ and $F_5TeNH_3^+$ analogues.[11] The additional fine structure observed on the quintet results from second-order transitions, which were confirmed by spectral simulation.

The ^{129}Xe NMR spectrum of $F_5SN(H)Xe^+$ is a singlet [$\Delta\nu_{1/2} = 128$ (150) Hz] at −2897 (−2956) ppm. The high ^{129}Xe

(22) Cady, G. H.; Eggers, D. F.; Tittle, B. *Proc. Chem. Soc.* **1963**, 65–66.
(23) See ref 11 and references therein.
(24) Merrill, C. I.; Williamson, S. M.; Cady, G. H.; Eggers, D. F., Jr. *Inorg. Chem.* **1962**, *1*, 215–219.

shielding places the Xe−N bond among the most covalent of Xe–N bonds,[25] but it is considerably less shielded than ^{129}Xe in $C_6F_5Xe^+$ (–3831 ppm, HF solvent, –40 °C).[26] The ^{129}Xe shielding is very similar to that in $F_5TeN(H)Xe^+$ (–2841 ppm, HF solvent, –45 °C; –2902 ppm, BrF_5 solvent, –48 °C), and both $F_5TeN(H)Xe^+$ and $F_5SN(H)Xe^+$ are considerably more shielded than the ^{129}Xe resonances of $XeN(SO_2F)_2^+$ (–1943 ppm, SbF_5 solvent, 25 °C),[5] $F_3S{\equiv}NXeF^+$ (–1652 ppm, HF solvent, –20 °C; –1661 ppm, BrF_5 solvent, –60 °C),[12] isovalent F_5TeOXe^+ (–1472 ppm, SbF_5 solvent, 5 °C),[27] and XeF^+ (–574 ppm, SbF_5 solvent, 25 °C).[28] As in the case of $F_5TeN(H)Xe^+$,[11] the ^{129}Xe shielding may be used as a gauge of L-group electronegativity and Xe–E bond covalency (L is an electronegative ligand and E is a second row ligand atom), and the shielding increases (group electronegativity decreases) with Xe–E bond covalency for the series of LXe^+ cations, that is, Xe–C > Xe–N > Xe–O > Xe–F. The ^{129}Xe–^{14}N coupling is not observed in $F_5SN(H)Xe^+$ because of quadrupolar relaxation of ^{14}N resulting from the low symmetry (high electric field gradient) at the nitrogen nucleus. The broad ^{129}Xe line widths of $F_5SN(H)Xe^+$ recorded at 11.7440 T precluded observation of the long-range couplings to xenon, namely, $^2J(^{129}Xe–^1H)$, $^3J(^{129}Xe–^{19}F_{ax})$, and $^3J(^{129}Xe–^{19}F_{eq})$, which are presumably, in large measure, attributable to the relaxation of ^{129}Xe by shielding anisotropy (SA), and also were not observed for $F_5TeN(H)Xe^+$.[11]

The ^{1}H NMR spectrum of $F_5SN(H)Xe^+$ consisted of a singlet at 9.57 ppm in BrF_5 supercooled to –70 °C, but the coupling to ^{14}N was not observed, as a result of quadrupolar relaxation. Failure to observe the $^2J(^{129}Xe–^1H)$ coupling is also attributed to broadening of the ^{129}Xe satellites as a result of a significant SA contribution to T_1 at the high external field strength used to obtain the ^{1}H NMR spectra.

X-ray Crystal Structure of $[F_5SN(H)Xe][AsF_6]$. A summary of the refinement results and other crystallographic information are provided in Table 2. Important bond lengths and angles for $[F_5SN(H)Xe][AsF_6]$ are listed in Table 3 along with calculated values for the $F_5SN(H)Xe^+$ and $F_5SNH_3^+$ cations. The $[F_5SN(H)Xe][AsF_6]$ unit cell is isomorphous with that of $[F_5TeN(H)Xe][AsF_6]$[11] and belongs to the $P\bar{1}$ space group. The sulfur analogue has a unit cell volume that is 27.6(6) Å^3 smaller than that of the tellurium analogue.

The $F_5SN(H)Xe^+$ cation and the AsF_6^- anion form an ion pair by interaction through a Xe---F–As fluorine bridge (Figure 2a) in which the AsF_6^- anion is distorted from O_h to approximate C_{4v} local symmetry. The symmetry lowering experienced by the anion is shown in the crystal structure to be very close to an axial distortion in which the four equatorial As–F bonds are equal to within $\pm 3\sigma$ and the As–F bond trans to the elongated bridging As---F bond is equal to the equatorial As–F bonds within $\pm 3\sigma$, thus preserving the 4-fold principal axis.

Table 2. Summary of Crystal Data and Refinement Results for $[F_5SN(H)Xe][AsF_6]$

	$[F_5SN(H)Xe][AsF_6]$
empirical formula	$HAsF_{11}NSXe$
space group (No.)	$P\bar{1}$ (2)
a (Å)	5.3248(9)
b (Å)	7.100(1)
c (Å)	11.877(2)
α (deg)	87.551(5)
β (deg)	83.398(5)
γ (deg)	86.278(6)
V (Å^3)	444.8(1)
molecules/unit cell	2
mol wt (g mol^{-1})	462.275
D_{calcd} (g cm^{-3})	3.452
T (°C)	−173
μ (mm^{-1})	7.95
wavelength (Å)	0.71073
final agreement factors[a]	$R_1 = 0.0218$
	$wR_2 = 0.0481$

[a] R_1 is defined as $\sum||F_o| - |F_c||/\sum|F_o|$ for $I > 2\sigma(I)$; wR_2 is defined as $[\sum[w(F_o^2 - F_c^2)^2]/\sum w(F_o^2)^2]^{1/2}$ for $I > 2\sigma(I)$.

In $[F_5SN(H)Xe][AsF_6]$, the Xe–N (2.069(4) Å) and Xe---F(6) (2.634(4) Å) bond lengths are somewhat longer than their counterparts in $[F_5TeN(H)Xe][AsF_6]$ (2.044(4) and 2.580(3), respectively), while the Xe–N–H, N–Xe---F(6), and S/Te–N–Xe angles are all equal within experimental error, and the As–F(6) bond lengths (1.759(4) Å and 1.740(4) Å, respectively) are similar. The longer Xe–N and Xe---F(6) bond lengths in the sulfur analogue are offset by the expected shorter S–N (1.761(4) Å), S–F_{ax} (1.559(3) Å), and average S–F_{eq} (1.573(4) Å) bond lengths when compared with the Te–N (1.982(5) Å), Te–F_{ax} (1.791(4) Å), and average Te–F_{eq} (1.811(5) Å) bond lengths of $[F_5TeN(H)Xe][AsF_6]$ and account for the smaller unit cell volume of the sulfur analogue.

The contributions to the total bond valency of xenon in $[F_5SN(H)Xe][AsF_6]$ and $[F_5TeN(H)Xe][AsF_6]$ have been determined for the Xe–N bond, the Xe---F contact to the AsF_6^- anion of the ion pair, and all long Xe---F contacts that fall within the sum of the xenon and fluorine van der Waals radii (3.63 Å)[29] according to the method described by Brown[30] (Table S1). The xenon atom in $[F_5SN(H)Xe][AsF_6]$ has six long Xe---F contacts [Xe---F(6A), 3.342 Å; Xe---F(6B), 3.387 Å; Xe---F(5A), 3.271 Å; Xe---F(2A), 3.267 Å; Xe---F(1A), 3.376 Å; and Xe---F(1B), 3.225 Å], compared to four Xe---F contacts in the tellurium salt which, in the latter case, are somewhat shorter in order to achieve a similar total bond valency at Xe. The longer Xe–N and Xe---F bridge bonds of the sulfur analogue have a bond valency sum at Xe (1.020 v.u.) that is 0.088 bond valence units less than that of the tellurium analogue (1.108 v.u.). The six long Xe---F contacts in the sulfur salt, however, have a bond valency sum that is 0.038 bond valency units greater than the sum for the four long Xe---F contacts of the tellurium analogue 0.148 v.u. The two additional long contacts in $[F_5SN(H)Xe][AsF_6]$ partly compensate for the

(25) Gerken, M.; Schrobilgen, G. J. *Coord. Chem. Rev.* **2000**, *197*, 335–395.
(26) Koppe, K.; Bilir, V.; Frohn, H. J.; Mercier, H. P. A.; Schrobilgen, G. J. *Inorg. Chem.* **2007**, *46*, 9425–9437.
(27) Keller, N.; Schrobilgen, G. J. *Inorg. Chem.* **1981**, *20*, 2118–2129.
(28) Schrobilgen, G. J.; Holloway, J. H.; Granger, P.; Brevard, C. *Inorg. Chem.* **1978**, *17*, 980–987.
(29) Bondi, A. *J. Phys. Chem.* **1964**, *68*, 441–451.
(30) Brown, I. D. *The Chemical Bond in Inorganic Chemistry*; Oxford University Press: Oxford, U.K., 2002.

Table 3. Experimental Geometry for $[F_5SN(H)Xe][AsF_6]$ and Calculated Geometries for $F_5SN(H)Xe^+$ and $F_5SNH_3^+$[a]

	Bond Lengths (Å)				
	$F_5SN(H)Xe^+$ (C_1)			$F_5SNH_3^+$ (C_1)	
	exptl	calcd[b]		calcd[c]	
		MP2	SVWN	MP2	SVWN
Xe(1)−N(1)	2.069(4)	2.065	2.095		
N(1)−S(1)	1.761(4)	1.822	1.805	1.853	1.853
N(1)−H(1)	0.801[d]	1.028	1.042	1.023	1.045
N(1)−H(2)				1.023	1.044
N(1)−H(3)				1.022	1.044
S(1)−F(1)	1.559(3)	1.544	1.548	1.531	1.561
S(1)−F(2)	1.565(3)	1.578	1.589	1.567	1.595
S(1)−F(3)	1.578(3)	1.578	1.583	1.567	1.594
S(1)−F(4)	1.578(3)	1.591	1.596	1.567	1.594
S(1)−F(5)	1.571(3)	1.561	1.569	1.567	1.594
Xe(1)---F(6)	2.634(3)		2.251		
	Bond Angles (deg)				
	$F_5SN(H)Xe^+$ (C_1)			$F_5SNH_3^+$ (C_1)	
	exptl	calcd[b]		calcd[c]	
		MP2	SVWN	MP2	SVWN
Xe(1)−N(1)−S(1)	115.3(2)	115.0	113.5		
Xe(1)−N(1)−H(1)	107.2[d]	101.2	101.1		
S(1)−N(1)−H(1)	106.9[d]	104.9	104.5	110.0	109.0
S(1)−N(1)−H(2)				109.2	108.8
S(1)−N(1)−H(3)				109.4	108.7
N(1)−S(1)−F(1)	176.7(2)	177.4	176.6	179.2	179.2
N(1)−S(1)−F(2)	87.4(2)	86.1	85.7	87.9	88.0
N(1)–S(1)–F(3)	94.0(2)	89.8	90.3	86.2	86.5
N(1)–S(1)–F(4)	88.5(2)	91.6	92.2	87.2	87.0
N(1)–S(1)–F(5)	90.7(2)	86.4	85.9	87.0	87.4
F(1)–S(1)–F(2)	89.6(2)	92.1	92.0	92.9	92.8
F(1)–S(1)–F(3)	89.0(2)	91.9	92.1	92.9	92.8
F(1)–S(1)–F(4)	90.2(2)	90.3	90.4	92.9	92.8
F(1)–S(1)–F(5)	90.5(2)	91.6	91.6	92.9	92.8
F(2)–S(1)–F(3)	178.4(2)	175.9	175.9	174.1	174.4
F(2)–S(1)–F(4)	89.2(2)	89.8	89.9	89.7	89.8
F(2)–S(1)–F(5)	90.5(2)	90.1	89.9	89.7	89.7
F(3)–S(1)–F(4)	90.0(2)	89.6	89.8	90.0	90.0
F(3)–S(1)–F(5)	90.2(2)	90.2	90.3	90.0	89.9
F(4)–S(1)–F(5)	179.2(2)	178.0	178.1	174.1	174.4

[a] The labels correspond to those used in Figure 2. [b] (SDB-)cc-pVTZ basis set. [c] cc-pVTZ basis set. [d] The hydrogen position was calculated by use of a riding model; therefore, no error is given.

loss of bond valency that results from the longer Xe---F bridge and Xe–N bonds. Thus, the total bond valency of Xe in $F_5SN(H)Xe^+$ (1.206 v.u.) is only 0.050 bond valence unit less than that of the tellurium salt (1.256 v.u.). These additional long contacts also correlate with closer packing in the $F_5SN(H)Xe^+$ salt, which is manifested by the smaller crystallographic unit cell volume observed for this salt. The long fluorine contacts to xenon in $F_5SN(H)Xe^+$ avoid the torus of electron density around xenon(II).[31] These contacts may also contribute to distortion of the N–Xe---F angle from the expected linear AX_2E_3 VSEPR arrangement; however, a similar deviation from linearity was obtained in the energy-minimized gas-phase geometry (Table S2; see Computational Results), and for F–Ng---F (Ng = Kr or Xe) in $Kr_2F_3^+$,[32] $Xe_2F_3^+$,[33] and $[KrF][MF_6]$ (M = As, Sb, or Bi),[32] and therefore may not be wholly attributable to crystal packing. The Xe---F(6)–As bridge bond angle (127.2(1)°) is comparable to that in $[F_5TeN(H)Xe][AsF_6]$ (128.1(2)°)[11] and is consistent with the bent geometry predicted by the VSEPR model and with the observed range of Ng---F–As (Ng = Xe, Kr) angles in $[XeF][AsF_6]$ (134.8(2)°),[34] $HF\cdot[HO-TeF_4-OXe][AsF_6]$ (133.0(4)°),[35] $[KrF][AsF_6]$ (133.7(1)°),[32] $[Kr_2F_3][AsF_6]\cdot[KrF][AsF_6]$ (127.5(3)°),[32] and $[C_6F_5Xe][AsF_6]$ (128.7(3)° and 126.4(3)°).[36]

Raman Spectroscopy. The Raman spectra of $[F_5SNH_3][AsF_6]$ (Figure 3) and $[F_5SN(H)Xe][AsF_6]$ (Figure 4) were assigned by comparison with those of $F_5TeNH_3^+$,[11] $F_5TeN(H)Xe^+$,[11] F_5TeOXe^+,[27,37] SF_6,[38,39] and F_5SCl[40] (Tables

(31) Mercier, H. P. A.; Moran, M. D.; Sanders, J. C. P.; Schrobilgen, G. J.; Suontamo, R. J. *Inorg. Chem.* **2005**, *44*, 49–60.
(32) Lehmann, J. F.; Dixon, D. A.; Schrobilgen, G. J. *Inorg. Chem.* **2001**, *40*, 3002–3017.
(33) Fir, B. A.; Gerken, M.; Pointner, B. E.; Mercier, H. P. A.; Dixon, D. A.; Schrobilgen, G. J. *J. Fluorine Chem.* **2000**, *105*, 159–167.
(34) Zalkin, A.; Ward, D. L.; Biagioni, R. N.; Templeton, D. H.; Bartlett, N. *Inorg. Chem.* **1978**, *17*, 1318–1322.
(35) Turowsky, L.; Seppelt, K. *Inorg. Chem.* **1990**, *29*, 3226–3228.
(36) Frohn, H.-J.; Klose, A.; Schroer, T.; Henkel, G.; Buss, V.; Opitz, D.; Vahrenhorst, R. *Inorg. Chem.* **1998**, *37*, 4884–4890.
(37) Fir, B. A.; Mercier, H. P. A.; Sanders, J. C. P.; Dixon, D. A.; Schrobilgen, G. J. *J. Fluorine Chem.* **2001**, *110*, 89–107.
(38) Claassen, H. H.; Goodman, G. L.; Holloway, J. H.; Selig, H. *J. Chem. Phys.* **1970**, *53*, 341–348.

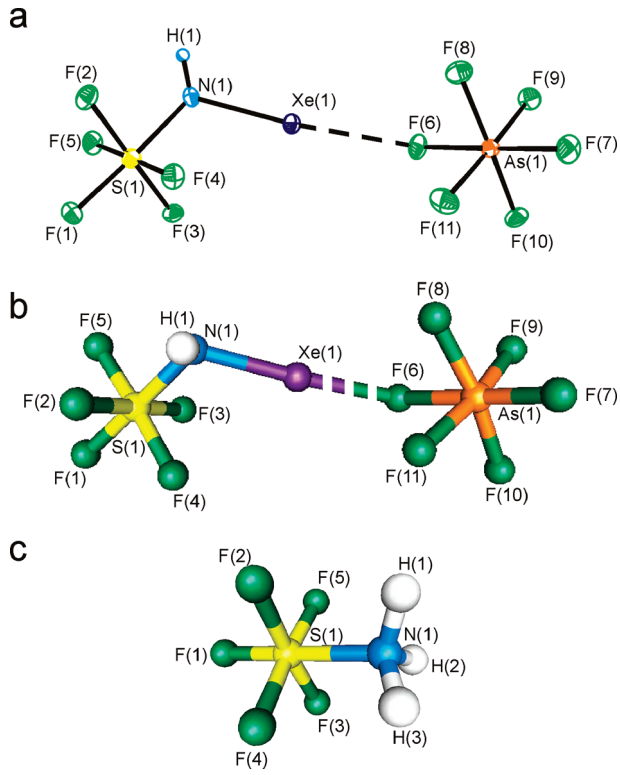

Figure 2. (a) X-ray crystal structure of $[F_5SN(H)Xe][AsF_6]$; thermal ellipsoids are shown at the 50% probability level. (b) Calculated geometry of $[F_5SN(H)Xe][AsF_6]$. (c) Calculated geometry of the $F_5SNH_3^+$ cation.

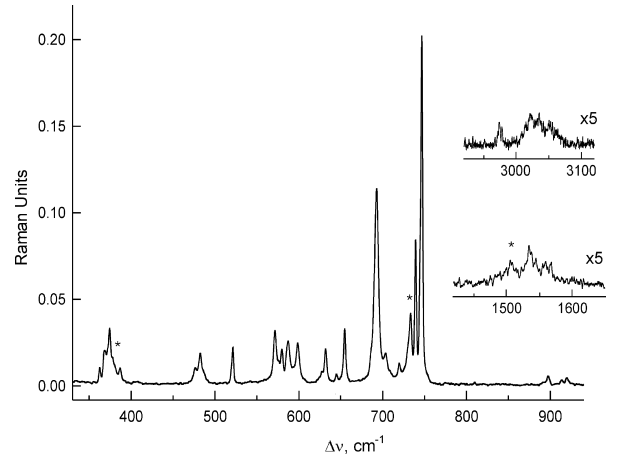

Figure 3. Raman spectrum of $[F_5SNH_3][AsF_6]$ recorded at –160 °C using 1064-nm excitation; symbols denote FEP sample tube lines (*).

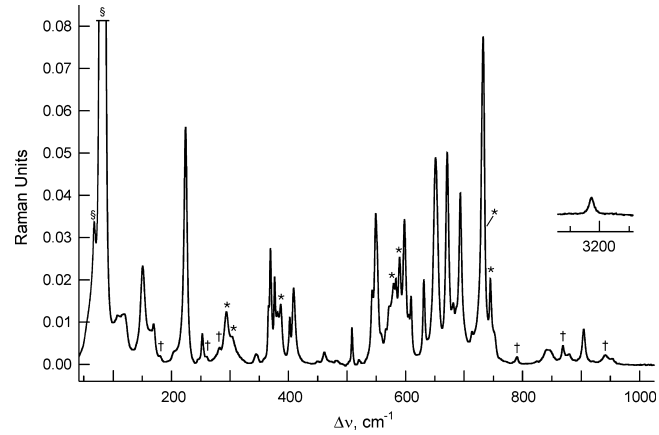

Figure 4. Raman spectrum of $[F_5SN(H)Xe][AsF_6]$ recorded at –45 °C using 1064-nm excitation; symbols denote FEP sample tube lines (*), lines arising from a minor impurity (†), and an instrumental artifact (§).

4 and 5), and by comparison with the calculated frequencies derived for the gas-phase energy-minimized geometries of $F_5SNH_3^+$, $F_5SN(H)Xe^+$, and the $[F_5SN(H)Xe][AsF_6]$ ion pair (see Computational Results). The vibrational modes of the uncoordinated AsF_6^- anion were assigned by comparison with those of $[O_2][AsF_6]$,[41] $[HC{\equiv}NXeF][AsF_6]$,[8] $[F_3S{\equiv}NXeF][AsF_6]$,[12] and $[F_5TeNH_3][AsF_6]$,[11] and the modes of the distorted fluorine-bridged AsF_6^- anion were assigned by comparison with those of $[F_5TeN(H)Xe][AsF_6]$,[11] $[F_5TeOXe][AsF_6]$,[37] $[XeF][AsF_6]$,[42] and $[KrF][AsF_6]$.[43] Calculated frequencies appearing in parentheses were obtained at the MP2/SVWN levels, respectively, except for the ion pair, which could only be optimized at the SVWN level (Table S3). The vibrational frequencies of SF_6 and F_5SCl were chosen as benchmarks for the F_5S-group frequencies of $F_5SNH_3^+$ and $F_5SN(H)Xe^+$ (Table S4; see Computational Results).

(a) $[F_5SNH_3][AsF_6]$. In the absence of a refined crystal structure, it was not possible to carry out a factor-group analysis, which might account for the splittings observed on the majority of the cation and anion Raman bands. The 24 vibrational modes of $F_5SNH_3^+$ were assigned under C_1 point symmetry and belong to A irreducible representations, all of which are Raman- and infrared-active. The 15 vibrational modes of AsF_6^- were assigned under O_h symmetry and belong to the irreducible representations $A_{1g} + E_g + T_{2g} + 2T_{1u} + T_{2u}$, where the A_{1g}, E_g, and T_{2g} modes are Raman-active and the T_{1u} modes are infrared-active. The formally Raman-inactive T_{1u} mode was, however, observed in the Raman spectrum as a weak band at 387 cm^{-1}.

The asymmetric NH_3 stretches at 3138 (3524/3310) and 3072 (3521/3307) cm^{-1}, the symmetric NH_3 stretch at 2939 (3402/3191) cm^{-1}, and the NH_3 bends at 1560 (1641/1569) and 1535 (1633/1552) cm^{-1} were overestimated by the calculations, which was also observed for $F_5TeNH_3^+$.[11] The S–N stretch couples with the equatorial SF_4 in-phase breathing mode at 739, 745, 747 cm^{-1} (757/697 cm^{-1}) and with the equatorial SF_4 out-of-phase, out-of-plane bend at 576 cm^{-1} (574/508 cm^{-1}), contrasting with the Te–N stretch of $F_5TeNH_3^+$, which is not significantly coupled. The out-of-phase trans equatorial SF_2 stretching modes are coupled to NH_3 rocking modes, whereas the axial S–F stretch is not coupled. All of the bands involving S–F stretches fall into the range 645–920 cm^{-1} (669–970/642–924 cm^{-1}), and those involving SF_5 bending modes occur in the range 362–632 cm^{-1} (316–613/282–563 cm^{-1}), and these have frequencies

(39) Weinstock, B.; Goodman, G. L. *Adv. Chem. Phys.* **1965**, *9*, 169–316.
(40) Marsden, C. J.; Bartell, L. S. *Inorg. Chem.* **1976**, *15*, 3004–3009.
(41) Naulin, C.; Bougon, R. *J. Chem. Phys.* **1976**, *64*, 4155–4158.
(42) Gillespie, R. J.; Landa, B. *Inorg. Chem.* **1973**, *12*, 1383–1388.
(43) Gillespie, R. J.; Schrobilgen, G. J. *Inorg. Chem.* **1976**, *15*, 22–31.

Table 4. Raman Vibrational Frequencies, Intensities, and Assignments for $[F_5SNH_3][AsF_6]$ and Calculated Vibrational Frequencies and Intensities for $F_5SNH_3^+$

freq, cm^{-1}							
$[F_5SNH_3][AsF_6]$	$F_5SNH_3^+$						
	calcd[b]				assgnts[c]		
exptl[a]	MP2		SVWN		$F_5SNH_3^+$ (C_1)	AsF_6^- (O_h)	
3138 (2) br	3524	(20) [163]	3310	(26) [178]	ν(NH2 – NH3)		
3072 (2) br	3521	(20) [163]	3307	(27) [178]	ν(NH2 + NH3) – ν(NH1)		
2939 (2) br	3402	(60) [103]	3191	(64) [110]	ν(NH1 + NH2 + NH3)		
1560 (2) br	1641	(3) [40]	1569	(4) [43]	ρ_t(H2NH3) + δ(NH1) wag – o.o.p.		
1535 (3) br	1633	(3) [42]	1552	(4) [43]	δ(H2NH3) + δ(NH1) wag – i.p.		
n.o.	1449	(<1) [163]	1360	(<1) [169]	δ(NH_3) inv		
n.o.	1066	(<1) [261]	1023	(<1) [256]	ν(SF4 – SF5) – NH_3 rock		
n.o.	1064	(<1) [261]	1022	(<1) [256]	ν(SF2 – SF3) – NH_3 rock		
920 (2)	970	(<1) [345]	924	(1) [295]	ν(SF1)		
914 (2)	914	(1) [115]	870	(1) [91]	ν(SF4 – SF5) + NH_3 rock		
898 (3)	914	(1) [114]	868	(1) [90]	ν(SF2 – SF3) + NH_3 rock		
747 (100)							
745 sh	757	(14) [5]	697	(19) [1]	ν(SF2 + SF3) + ν(SF4 + SF5) + ν(SN)		
739 (42)							
720 (7)							
704 (10)						ν_1 (A_{1g})	
693 (57)							
655 (16)							
645 (3)	669	(3) [<1]	642	(4) [<1]	ν(SF2 + SF3) – ν(SF4 + SF5)		
632 (11)							
628 sh	613	(1) [94]	563	(4) [50]	δ(SF_{4eq}) o.o.p.		
599 (12)							
587 (13)						ν_2 (E_g)	
580 (11)							
576 sh	574	(<1) [19]	508	(4) [23]	ν(SN) + δ(F2SF3) + δ(F4SF5)		
572 (16)	574	(<1) [19]	505	(<1) [14]	δ(F1SN) + δ(F2SF3)		
521 (11)	527	(2) [<1]	504	(2) [18]	δ(F1SN) + δ(F4SF5)		
518 sh	518	(8) [1]	464	(2) [<1]	δ(F3SF4) + δ(F2SF5)		
487 sh	458	(1) [<1]	404	(1) [1]	δ(F1SF5) + δ(F4SN)		
482 (10)							
476 (3)	456	(1) [<1]	402	(1) [1]	δ(F1SF2) + δ(F5SN)		
387 (5)						ν_4 (T_{1u})	
378 sh							
374 (17)						ν_5 (T_{2g})	
368 sh	330	(<1) [<1]	293	(<1) [<1]	δ(F2SF3) – δ(F4SF5)		
362 (5)	320	(<1) [9]	286	(<1) [10]	δ(F1SN) o.o.p.		
	316	(<1) [10]	282	(1) [10]	δ(F1SN) i.p.		
n.o.	4	(<1) [1]	18	(<1) [1]	NH_3 torsion		

[a] Values in parentheses denote experimental relative Raman intensities, and abbreviations denote broad (br), shoulder (sh), and not observed (n.o.). [b] cc-pVTZ basis set. Calculated infrared intensities (in km mol^{-1}) are given in brackets, and calculated Raman intensities (in $Å^4$ amu^{-1}) are given in parentheses. [c] The atom numbering corresponds to that used in Figure 2, and abbreviations denote out-of-plane (o.o.p.) and in-plane (i.p.) (the plane is defined by the S, N, and H1 atoms), inversion (inv), twist (ρ_t), and four equatorial fluorines (F_{4eq}).

similar to those of SF_6 (615–940 and 347–525 cm^{-1}) and F_5SCl (602–909 and 271–579 cm^{-1}).[40] The NH_3 torsion, predicted at (4/18 cm^{-1}), could not be observed.

(b) $[F_5SN(H)Xe][AsF_6]$. The $F_5SN(H)Xe^+$ cation (gas-phase and crystallographic symmetries optimized to C_1 symmetry) possesses 21 fundamental vibrational modes belonging to A irreducible representations, which are both Raman- and infrared-active. The fluorine bridge interaction lowered the O_h symmetry of the anion (see X-ray Crystal Structure of $[F_5SN(H)Xe][AsF_6]$) so that additional lines in the vibrational spectra were observed. Such symmetry lowering in hexafluoro anions of group 15 is oftentimes approximated as C_{4v} symmetry,[44] and the vibrational spectra are assigned under this or a lower symmetry (C_{2v}, C_s, or C_1). The distorted anion in the structural unit possesses 15 fundamental vibrational modes under approximate C_{4v} symmetry belonging to the irreducible representations $4A_1 + 2B_1 + B_2 + 4E$, all of which are Raman-active, and the A_1 and E modes are infrared-active. In practice, 9 of the 11 vibrational bands expected under C_{4v} symmetry were observed (correlations to O_h symmetry are given in square brackets), namely, 681 (A_1) and 693, 714 (E) [T_{1u}], 598 (B_1) and 609 (A_1) [E_g], 402 (A_1) and 409 (A_1) [T_{1u}], and 369 (E) and 376 (B_2) [T_{2g}] cm^{-1}. Factor-group analyses correlating the cation (C_1) and anion (C_{4v}) symmetries to their crystal site symmetries (C_1) and to the unit cell symmetry (C_i) are provided in Table S5. The A irreducible representations of the cation are maintained under C_1 site symmetry, while the doubly degenerate E modes of the anion are split as a result of site symmetry lowering. Both the cation and anion modes are split into Raman-active A_g and infrared-active A_u components under C_i crystal symmetry, giving the potential to observe 21 bands for the cation and 15 bands for the anion. As predicted, no additional splittings of the 19 observed cation bands and 11 observed anion bands occurred in the Raman spectrum under the crystal symmetry.

The calculated vibrational frequencies for the $[F_5SN(H)Xe][AsF_6]$ ion pair and for the isolated $F_5SN(H)Xe^+$ and AsF_6^- ions are generally in good agreement with the

(44) See ref 32 and references therein.

Table 5. Raman Vibrational Frequencies, Intensities, and Assignments for $[F_5SN(H)Xe][AsF_6]$, and Calculated Vibrational Frequencies and Intensities for $F_5SN(H)Xe^+$

freq, cm^{-1}							
$[F_5SN(H)Xe][AsF_6]$	$F_5SN(H)Xe^+$						
	calcd[b]				assgnts[c]		
exptl[a]	MP2		SVWN		$F_5SN(H)Xe^+$ (C_1)	AsF_6^- (C_{4v})	
3186 (7)	3421	(38) [92]	3287	(40) [103]	ν(NH)		
n.o.	1328	(<1) [25]	1230	(1) [28]	δ(NH) wag – i.p.		
954 (2) br	980	(1) [277]	946	(5) [227]	δ(SNH)		
904 (14)	952	(2) [253]	921	(3) [261]	ν(SF4 – SF5) + ν(SF1)		
879 (4)	936	(2) [395]	902	(11) [303]	ν(SF2 – SF3) + ν(SF1)		
844 (6) br	888	(2) [145]	856	(5) [135]	δ(NH) wag – o.o.p.		
732 (58)	737	(7) [8]	701	(8) [5]	ν(SF2 + SF3) + ν(SF4 + SF5) + ν(SN)		
714 (10)						ν_8 (E)	
693 (69)							
681 (22)						ν_1 (A_1)	
671 (86)	661	(16) [10]	627	(4) [2]	ν(SF2 + SF3) – ν(SF4 + SF5)		
651 (83)	650	(4) [3]	586	(37) [>1]	ν(XeN) – ν(SN)		
631 (32)	606	(1) [130]	577	(4) [134]	$\delta(SF_{4eq})$ o.o.p.		
609 (26)						ν_2 (A_1)	
598 (59)						ν_5 (B_1)	
549 (61)	595	(2) [12]	566	(1) [13]	δ(F2SF3) + δ(NSF4) – δ(F1SF5)		
543 (29)	574	(<1) [18]	538	(1) [14]	δ(F1SF4) – δ(F3SF5)		
520 (4) br	535	(5) [13]	512	(3) [10]	ν(XeN) + ν(SN) + δ(F1SF4) + δ(F3SF4) – δ(F2SF5)		
508 (17)	511	(1) [<1]	479	(2) [<1]	δ(F3SF5) + δ(F2SF4)		
461 (4) br			420	(17) [109][d]	ν(Xe--F6)[d]		
409 (33)	446	(1) [6]	415	(<1) [6]	ρ_t(F1SN) + ρ_w(F2SF4) – ρ_w(F3SF5)	ν_4 (A_1)	
402 (20)						ν_3 (A_1)	
376 (37)						ν_7 (B_2)	
369 (49)						ν_9 (E)	
366 (24)	407	(2) [3]	382	(2) [4]	δ(F1SN) + ρ_w(F2SF5) – ρ_w(F3SF4)		
345 (4) br	338	(<1) [1]	316	(<1) [1]	ρ_t(F2SF5) – ρ_t(F3SF4)		
252 (13)	285	(1) [4]	254	(1) [4]	δ(F1SN) o.o.p.		
224 (100)	222	(3) [<1]	207	(4) [<1]	ν(XeN) + $\rho_r(SF_5)$		
169 (14)			156	(1) [8][d]	coupled deformation mode of $[F_5SN(H)Xe][AsF_6]$[d]		
151 (37)	136	(1) [1]	125	(2) [1]	δ(XeNS)		
119 (14)			105	(1) [1][d]	coupled deformation modes of $[F_5SN(H)Xe][AsF_6]$[d]		
108 (14)			76	(1) [1][d]			
n.o.	56	(1) [1]	45	(2) [1]	torsion about Xe		

[a] Values in parentheses denote experimental relative Raman intensities, and abbreviations denote broad (br) and not observed (n.o.). [b] (SDB-)cc-pVTZ basis set. Calculated infrared intensities (in km mol^{-1}) are given in brackets, and calculated Raman intensities (in $Å^4$ amu^{-1}) are given in parentheses. [c] The atom numbering corresponds to that used in Figure 2, and abbreviations denote in-plane (i.p.) and out-of-plane (o.o.p.; the plane is defined by Xe, N, and S atoms), twist (ρ_t), wag (ρ_w), rock (ρ_r), and four equatorial fluorines (F_{4eq}). [d] Values and mode descriptions are from the calculated ion pair; see Table S3 for a full frequency listing and assignments.

experimental frequencies. The ion pair calculation shows that the cation and anion modes are not coupled except for the low-frequency deformation modes. The modes associated with the Xe---F–As bridge are, however, deemed to be less reliable because the geometrical parameters of the Xe---F–As bridge are not well reproduced for the calculated ion pair (see Computational Results).

Coupled ν(SN + XeN) and ν(SN – XeN) stretches were observed at 520 and 651 (535/512 and 650/586) cm^{-1}, respectively, compared with the coupled ν(TeN + XeN) and ν(TeN – XeN) stretches observed for $F_5TeN(H)Xe^+$ at 444 and 654 cm^{-1}.[11] The most intense band in the Raman spectrum of $[F_5SN(H)Xe][AsF_6]$ occurs at 224 (222/207) cm^{-1} and is assigned to the Xe–N stretch weakly coupled to a F_5S-group rock, whereas the corresponding low-frequency coupled mode was not observed for the tellurium analogue. Weak coupling between the Xe–N stretch and F_5S-group rock of $F_5SN(H)Xe^+$ may be the result of the larger mass difference between xenon and sulfur than between xenon and tellurium. The equatorial SF_4 symmetric breathing mode is weakly coupled with the S–N stretch and occurs at 732 cm^{-1} (737/701 cm^{-1}), as observed in $F_5SNH_3^+$ (739, 745, and 747 cm^{-1}). The broad band at 461 cm^{-1} could not be assigned by comparison with the modes calculated for the gas-phase $F_5SN(H)Xe^+$ cation and, consequently, was assigned to ν(Xe---F) by comparison with the frequency calculated for the ion pair (420 cm^{-1}), with the difference attributed to the underestimated Xe---F distance. This frequency is higher than that assigned to ν(Xe---F) in $[XeN(SO_2F)_2][AsF_6]$ (317 cm^{-1}),[5] $[XeOTeF_5][AsF_6]$ (365 cm^{-1}),[24,37] and $[XeF][AsF_6]$ (417 cm^{-1}).[42] The Xe–N–S bend is assigned to the strong band at 151 (136/125) cm^{-1}, which is higher than that of the Xe–N–Te bend in $F_5TeN(H)Xe^+$ (113 cm^{-1}).[11] The highest-frequency band, 3186 cm^{-1}, is assigned to ν(NH) (3421/3287 cm^{-1}) and is in good agreement with the N–H stretches in $F_5TeN(H)Xe^+$ (3146 cm^{-1}),[11] F_5TeNH_2 (symmetric, 3297 cm^{-1}; asymmetric, 3385 cm^{-1}),[11] $F_5TeNH_3^+$ (symmetric, 3018 cm^{-1}; asymmetric, 3110 cm^{-1}),[11] and $F_5SNH_3^+$ (symmetric, 2939 cm^{-1}; asymmetric, 3072, 3145 cm^{-1}).[45] The δ(SNH) bend, observed at 954 cm^{-1}, and δ(NH) wag, which was not observed, were calculated at 980/946 and 1328/1230 cm^{-1}, respectively, and are predicted to be weak. The experimental SF_5-group stretches (671–904 cm^{-1}) and bends (345–631 cm^{-1}) fall into ranges that are

(45) This work.

Table 6. Natural Bond Orbital (NBO) Charges, Valencies, and Bond Orders for $F_5SNH_3^{+a}$ and $F_5SN(H)Xe^{+b}$

	$F_5SNH_3^+$				$F_5SN(H)Xe^+$			
	charges		valencies		charges		valencies	
atom	MP2	SVWN	MP2	SVWN	MP2	SVWN	MP2	SVWN
Xe					1.01	0.98	0.57	0.61
H	0.45	0.47	0.63	0.68	0.40	0.43	0.71	0.72
N	−0.85	−0.90	2.39	2.52	−0.82	−0.82	1.82	1.90
S	2.61	2.51	3.67	3.93	2.58	2.48	3.67	3.91
F1	−0.39	−0.37	0.55	0.61	−0.41	−0.38	0.53	0.59
F2	−0.43	−0.42	0.49	0.55	−0.43	−0.41	0.49	0.54
F3	−0.43	−0.41	0.49	0.54	−0.45	−0.44	0.47	0.54
F4	−0.43	−0.42	0.49	0.55	−0.46	−0.45	0.45	0.51
F5	−0.43	−0.41	0.49	0.54	−0.42	−0.38	0.50	0.54

bond orders

	$F_5SNH_3^+$		$F_5SN(H)Xe^+$	
bond	MP2	SVWN	MP2	SVWN
Xe−N			0.58	0.60
N−H	0.65	0.69	0.71	0.72
S−N	0.55	0.56	0.64	0.68
S−F1	0.67	0.72	0.65	0.70
S−F2	0.61	0.66	0.60	0.63
S−F3	0.61	0.66	0.59	0.64
S−F4	0.61	0.66	0.58	0.62
S−F5	0.61	0.66	0.62	0.65

[a] cc-pVTZ basis set; the atom numbering corresponds to that used in Figure 2c. [b] (SDB-)cc-pVTZ basis set; the atom numbering corresponds to that used in Figure 2b.

similar to those of $F_5SNH_3^+$ and the benchmarks, SF_6 and F_5SCl (vide supra). The medium intensity modes at 108, 119, and 169 (76, 105, and 156) cm^{-1} are assigned to strongly coupled deformation modes associated with the ion pair, but the torsion about Xe, calculated at 56/45 cm^{-1}, could not be observed.

Computational Results. Electronic structure calculations were carried out for $F_5SNH_3^+$, $F_5SN(H)Xe^+$, and $[F_5SN(H)Xe][AsF_6]$ to aid in the vibrational assignments (see Raman Spectroscopy) and to gain insight into the structure and bonding of $F_5SNH_3^+$ and $F_5SN(H)Xe^+$. Comparisons of the calculated and experimental frequencies with those of the benchmarks, SF_6 and F_5SCl, showed that the SVWN calculations provided vibrational frequencies that were in better agreement than the MP2 calculations for the highest-frequency modes, the asymmetric SF_6 and equatorial SF_4 stretches of SF_6 and F_5SCl, respectively, whereas the MP2 calculations better reproduced the symmetric stretches and all of the F–S–F bending frequencies (Table S4).

(a) Calculated Geometries. Although close to C_s symmetry, both the MP2 and SVWN energy-minimized structures of the $F_5SNH_3^+$ and $F_5SN(H)Xe^+$ cations optimized to C_1 symmetry, as did the SVWN energy-minimized structure of the $[F_5SN(H)Xe][AsF_6]$ ion pair. These calculations reproduced the experimental geometric parameters of $F_5SN(H)Xe^+$ in the ion pair. The largest discrepancies occurred for the Xe---F–As fluorine bridge of the ion pair. The Xe---F(6) (2.251 Å) and As–F(6) (1.919 Å) fluorine-bridge bond lengths are under- and overestimated, respectively, when compared with the experimental values, 2.634(3) and 1.759(3) Å. The Xe---F–As angle, which was found to be bent in the low-temperature X-ray crystal structure (127.2(1)°) and is known to be influenced by crystal packing (see X-ray Crystal Structure), was significantly more bent (112.7°) for the calculated geometry. Similar differences were found for the $[F_5TeN(H)Xe][AsF_6]$ ion pair.[11] It is noteworthy that the calculated local symmetry of AsF_6^- in the $[F_5SN(H)Xe][AsF_6]$ ion pair is better approximated by C_{2v} symmetry than by the local C_{4v} symmetry used to assign the vibrational frequencies of AsF_6^- in the ion pair (see Raman Spectroscopy).

The calculated S–N bond length of $F_5SN(H)Xe^+$ is significantly shorter than that of $F_5SNH_3^+$ at both levels of theory. This trend was also observed for the experimental and calculated Te–N bond lengths in $F_5TeN(H)Xe^+$ and $F_5TeNH_3^+$,[11] whereas the S–F bond lengths of $F_5SN(H)Xe^+$ are slightly longer (MP2) or slightly shorter (SVWN) than in $F_5SNH_3^+$. It is not possible to discern significant differences in either the experimental or calculated Te–F bond lengths for the tellurium analogues.[11]

(b) Charges, Valencies, and Bond Orders. The Natural Bond Orbital (NBO) charges, valencies, and bond orders calculated using the MP2 and SVWN methods (SVWN values are given in parentheses) for $F_5SNH_3^+$ and $F_5SN(H)Xe^+$ are listed in Table 6. The formal positive charge of both cations chiefly resides on S, H, and Xe, with positive charges on S and H in $F_5SN(H)Xe^+$ that are slightly lower than the corresponding charges in $F_5SNH_3^+$. The Xe–N bond order [0.58 (0.60)] in $F_5SN(H)Xe^+$ and the decrease in N valency from $F_5SNH_3^+$ [2.39 (2.52)] to $F_5SN(H)Xe^+$ [1.82 (1.90)] also indicate significant covalent bonding between xenon and nitrogen. Slight decreases in the absolute charges on sulfur [2.58 (2.48)] and nitrogen [–0.82 (–0.82)] correspond to the greater S–N bond order [0.64 (0.68)] for $F_5SN(H)Xe^+$ when compared with that of $F_5SNH_3^+$ [0.55 (0.56)] [S charge: 2.61, (2.51); N charge: –0.85 (–0.90)]. The lower N–H bond order of $F_5SNH_3^+$ [0.65 (0.69)] compared with that of $F_5SN(H)Xe^+$ [0.71 (0.72)] and parallel decreases in absolute charges on H and N correspond to increased N–H bond covalency in $F_5SN(H)Xe^+$. There is little difference in the S–F bond orders or in the charges and valencies at sulfur and fluorine in $F_5SNH_3^+$ and $F_5SN(H)Xe^+$. The S–F_{eq} bond orders and F_{eq} valencies of both cations differ little from those of the benchmarks, SF_6 and F_5SCl, whereas the S–F_{ax} bond orders and the F_{ax} valencies are slightly higher in both cations.

Conclusions

The $F_5SN(H)Xe^+$ cation has been synthesized by reaction of XeF_2 with $F_5SNH_3^+$ in BrF_5 and aHF solvents, and by HF solvolysis of the recently reported $F_3S{\equiv}NXeF^+$ cation. The $F_5SN(H)Xe^+$ cation provides, in addition to $F_5TeN(H)Xe^+$, an example of xenon bonded to an sp^3-hybridized nitrogen, and the second example of a synthetic route that makes use of an ammonium ($F_5ChNH_3^+$, Ch = S or Te) cation as the synthetic precursor to a Xe–N bonded compound. The Xe–N bond length, calculated Xe–N bond order derived from the NBO analyses, high shielding of the ^{129}Xe NMR resonance, and empirical Xe–N bond valency derived from the crystal structure of $[F_5SN(H)Xe][AsF_6]$ are con-

sistent and place $F_5SN(H)Xe^+$ among the most covalent Xe–N bonded species presently known.

Experimental Section

Apparatus and Materials. All manipulations were carried out under strictly anhydrous conditions as previously described.[46] Literature methods were used to prepare $N{\equiv}SF_3$,[47] AsF_5,[48] XeF_2,[49] and $[F_3S{\equiv}NXeF][AsF_6]$[12] and to purify HF (Harshaw Chemical Co.),[8] BrF_5 (Ozark-Mahoning Co.),[49] and SO_2 (Canadian Liquid Air, Ltd.).[50]

$[F_5SNH_3][AsF_6]$. In a typical synthesis, a ¼-in. o.d. FEP (perfluorinated polyethylene, polypropylene copolymer) tube, fitted with a Kel-F valve, was connected to a FEP submanifold that was, in turn, connected to a stainless steel cylinder containing $N{\equiv}SF_3$. The cylinder was fitted with two Whitey valves separated by a ca. 5-cm length of ¼-in. o.d. stainless steel tubing to produce a volume (ca. 1.4 mL) which could be filled with an autogenous pressure of $N{\equiv}SF_3$. Condensation of successive 1.4 mL aliquots of $N{\equiv}SF_3$ allowed for a total of ca. 0.18 g (1.7 mmol) of $N{\equiv}SF_3$ to be metered into the reaction vessel. The reactor was then removed to a metal vacuum line that was, in turn, connected to a nickel vessel containing AsF_5. Excess AsF_5 (2.0 mmol) was condensed into the reaction vessel from the calibrated volume of the vacuum manifold at –196 °C, and the reaction mixture was warmed to –78 °C. The reaction was allowed to proceed, with occasional mixing, for ca. 1 h at –78 °C, forming $F_3S{\equiv}NAsF_5$ as a friable white solid. After removal of the excess AsF_5 by pumping at –78 °C for ca. 1 h, the sample was stored at –78 °C until it was characterized by Raman spectroscopy. The reactor was then connected to a FEP submanifold that was, in turn, connected to a Kel-F vessel containing aHF. Anhydrous HF was condensed onto $F_3S{\equiv}NAsF_5$ at –196 °C, and the reaction vessel was warmed to –78 °C, whereupon the HF liquified. The reaction mixture was warmed to 0 °C and was allowed to stand, with occasional mixing, for ca. 6 h, over which time the white solid dissolved and colorless featherlike crystals of $[F_5SNH_3][AsF_6]$ were deposited. After the removal of HF under a dynamic vacuum at –78 °C, the sample was stored at that temperature until it was characterized by Raman spectroscopy.

$[F_5SN(H)Xe][AsF_6]$. In a typical synthesis, ca. 1 mL of aHF was condensed onto $[F_3S{\equiv}NXeF][AsF_6]$ (0.1309 g, 0.2959 mmol) in a ¼-in. o.d. FEP reaction tube, fitted with a Kel-F valve, at –196 °C. The reaction vessel was initially warmed to –78 °C and then to –20 °C and was allowed to stand, with occasional mixing, for ca. 6 h, over which time the white solid slowly dissolved to form a yellow solution from which deep-yellow microcrystals deposited. After removal of the solvent under a dynamic vacuum at –78 °C, the sample was stored at that temperature until it was characterized by Raman spectroscopy.

The $F_5SN(H)Xe^+$ cation was also synthesized in a 4-mm o.d. FEP tube fused to a ¼-in. FEP tube which was fitted with a Kel-F valve that contained $[F_5SNH_3][AsF_6]$ (0.0502 g, 0.1501 mmol) and a 2-fold excess of XeF_2 (0.0508 g, 0.3003 mmol). Anhydrous HF or BrF_5 (ca. 0.5 mL) was statically distilled onto the sample at –196 °C, and the reaction vessel was initially warmed to –78 °C and then to –20 °C just prior to characterization by low-temperature multi-NMR spectroscopy.

Crystal Growth. (a) $[F_5SN(H)Xe][AsF_6]$. Anhydrous HF (ca. 1 mL) was condensed onto $[F_3S{\equiv}NXeF][AsF_6]$ (0.1186 g, 0.2681 mmol) at –196 °C that had been synthesized in situ in one arm of a ¼-in. o.d. FEP T-shaped reactor fitted with a Kel-F valve. The reactor was warmed to –78 °C and pressurized to 1 atm with dry nitrogen before warming to –20 °C, where the reaction was allowed to proceed for ca. 4 h, over which time the white solid slowly dissolved and the solution became deep yellow in color. Transparent yellow plates subsequently grew as the supernatant became colorless. While maintaining the reactor at –20 °C, the sample was attached to a vacuum line and the arm containing the solution was inclined ca. 5° from horizontal inside the glass Dewar of a crystal-growing apparatus[32] that had been previously adjusted to –20 °C. The temperature was lowered over a period of 1 h to –50 °C, where it was held for a further 30 min to allow for more complete crystallization. Transparent yellow plate-shaped crystals were isolated by decanting the solvent under dry nitrogen into the sidearm of the FEP vessel, which was immersed in liquid nitrogen. This was followed by lowering the sample temperature to –80 °C, evacuation, and heat-sealing the sidearm containing the supernatant at –196 °C. The crystalline sample was further dried under a dynamic vacuum at –80 °C before the crystallization vessel was back-filled with dry nitrogen and stored at –78 °C until a suitable crystal could be mounted for a single-crystal X-ray structure determination.

(b) $[F_5SNH_3][AsF_6]$. Anhydrous HF (ca. 1 mL) was condensed onto $[F_5SNH_3][AsF_6]$ (0.245 g, 1.70 mmol) at –196 °C that had been synthesized (vide supra) in situ in one arm of a ¼-in. o.d. FEP T-shaped reactor fitted with a Kel-F valve. The reactor was warmed to 0 °C to effect dissolution and initially gave a colorless solution. The reactor was placed inside the glass Dewar of a crystal-growing apparatus[32] that had been previously adjusted to 0 °C. This temperature was maintained, and over a period of 10 h, colorless plates slowly deposited that were isolated and transferred to a goniometer head as previously described.[51] Crystals of $[F_5SNH_3][AsF_6]$ were shown, by inspection under a stereomicroscope, to have striations in one plane that are associated with multiple crystal growth. This was confirmed by a low-angle data set collection as described below. Although unit cell parameters were reproducibly determined from six multiple crystals, a = 5.752(1) Å, b = 5.761(1) Å, c = 11.733(2) Å, α = 89.81(1)°, β = 89.93(1)°, and γ = 89.74(1)°, only a preliminary solution could be obtained in which bond length uncertainties exceeded 0.02 Å. This preliminary solution confirmed the expected gross structural features of the cation and anion and clearly indicated that the axial bond of the cation was longer than the remaining five bonds. A further crystallization attempt from SO_2 solvent also yielded multiple crystals that gave the same unit cell parameters. Attempts to characterize $[F_5SNH_3][AsF_6]$ by single-crystal X-ray diffraction have also proven unsuccessful in the hands of other workers.[52]

X-ray Crystallography. (a) Collection and Reduction of the X-ray Data. A crystal of $[F_5SN(H)Xe][AsF_6]$ having the dimensions 0.28 × 0.24 × 0.10 mm^3 was selected at –105 ± 3 °C for low-temperature X-ray structure determination and was mounted in a cold stream (–173 °C) on a goniometer head as previously described.[51]

The crystal was centered on a P4 Siemens diffractometer, equipped with a Siemens SMART 1K charge-coupled device (CCD) area detector that used the program SMART,[53] and a rotating anode

(46) Casteel, W. J., Jr.; Dixon, D. A.; Mercier, H. P. A.; Schrobilgen, G. J. *Inorg. Chem.* **1996**, *35*, 4310–4322.
(47) Mews, R.; Keller, K.; Glemser, O. *Inorg. Synth.* **1986**, *24*, 12–17.
(48) Emara, A. A. A.; Lehmann, J. F.; Schrobilgen, G. J. *J. Fluorine Chem.* **2005**, *126*, 1373–1376.
(49) Mercier, H. P. A.; Sanders, J. C. P.; Schrobilgen, G. J.; Tsai, S. S. *Inorg. Chem.* **1993**, *32*, 386–393.
(50) Collins, M. J.; Schrobilgen, G. J. *Inorg. Chem.* **1985**, *24*, 2608–2614.
(51) Gerken, M.; Dixon, D. A.; Schrobilgen, G. J. *Inorg. Chem.* **2000**, *39*, 4244–4255.
(52) Mews, R.; Žemva, B. Private communications.
(53) *SMART*, release 5.054; *SAINT*, release 056.001; Siemens Energy and Automation Inc.: Madison, WI, 1999.

using graphite-monochromated Mo Kα radiation ($\lambda = 0.710\ 73$ Å). The diffraction data collection consisted of a full ψ rotation at $\chi = 0°$ using (1040 + 40) 0.36° frames, followed by a series of short (80 frames) ω scans at various ψ and χ settings to fill the gaps. The crystal-to-detector distance was 5.016 cm, and the data collection was carried out in a 512 × 512 pixel mode using 2 × 2 pixel binning. Processing was carried out by using the program SAINT,[53] which applied Lorentz and polarization corrections to three-dimensionally integrated diffraction spots. The program SADABS[54] was used for the scaling of diffraction data, the application of a decay correction, and an empirical absorption correction based on redundant reflections.

(b) Solution and Refinement of the Structure. The XPREP program was used to confirm the unit cell dimensions and the crystal lattice. The final refinement was obtained by introducing anisotropic parameters for all the atoms, an extinction parameter, and the recommended weight factor. The maximum electron densities in the final difference Fourier maps were located around the heavy atoms. All calculations were performed with the SHELXTL package for structure determination, refinement, and molecular graphics.[55] A solution was obtained by direct methods which located the Xe and As atoms. Successive difference Fourier syntheses revealed the positions of the fluorine, nitrogen, and sulfur atoms. The position of the hydrogen atom in the $F_5SN(H)Xe^+$ cation was calculated [d(N–H) ≈ 0.82 Å; U(H) fixed to –1.5U(N)] and was then refined using DFIX restraints.

Nuclear Magnetic Resonance Spectroscopy. (a) NMR Sample Preparation. Samples of $[F_5SNH_3][AsF_6]$ and $[F_5SN(H)Xe][AsF_6]$ (ca. 50 mg each) were prepared in 4-mm o.d. FEP tubes fused to ¼-in. FEP tubing which were fitted with Kel-F valves that contained $F_3S{\equiv}NAsF_5$ (41 mg) and $[F_3S{\equiv}NXeF][AsF_6]$ (48 mg), respectively. The NMR tubes were connected to a FEP submanifold that was, in turn, connected through a Kel-F valve to a Kel-F storage vessel containing aHF. The FEP submanifold was connected to a metal vacuum line, and ca. 0.5 mL of aHF was statically distilled onto the starting materials at –196 °C. The NMR samples were then heat-sealed under dynamic vacuum and stored at –196 °C until their NMR spectra could be obtained. Samples were dissolved just prior to data acquisition at or below the temperature used to record their spectra. When obtaining low-temperature spectra, the 4-mm o.d. FEP tubes were inserted into a 5-mm o.d. thin-wall precision glass NMR tube (Wilmad).

(b) NMR Instrumentation and Spectral Acquisitions. Proton, ^{19}F, and ^{129}Xe nuclear magnetic resonance spectra were recorded unlocked (field drift <0.1 Hz h^{-1}) on a Bruker DRX-500 spectrometer equipped with an 11.744-T cryomagnet. The NMR probe was cooled using a nitrogen flow and variable-temperature controller (BVT 3000).

The ^{19}F (^1H) NMR spectra were acquired using a 5-mm combination $^1H/^{19}F$ probe operating at 470.592 (500.138) MHz. The spectra were recorded in 32K memories, with spectral width settings of 24 (6.8) kHz and acquisition times of 1.39 (2.42) s, and were zero-filled to 64K, yielding data point resolutions of 0.36 (0.21) Hz/data point. Relaxation delays of 0.10 (2.5) s were applied, and 1600 (8) transients were accumulated.

The ^{129}Xe NMR spectra were obtained using a 5-mm broad-band inverse probe operating at 138.086 MHz. The spectra were recorded in 32K memories, with spectral width settings of 97.1 kHz and acquisition times of 0.17 s, and were zero-filled to 64K, yielding data point resolutions of 2.96 Hz/data point. Relaxation delays of 0.10 s were applied, and 32 000 transients were accumulated.

Pulse widths, corresponding to a bulk magnetization tip angle of approximately 90°, were 2.0 (^1H), 8.5 (^{19}F), and 10.0 (^{129}Xe) μs. Line broadenings of 0 (^1H), 0.10 (^{19}F) and 5.0 (^{129}Xe) Hz were used in the exponential multiplications of the free induction decays prior to their Fourier transformations.

The ^1H, ^{19}F, and ^{129}Xe spectra were referenced externally at 30 °C to samples of neat $(CH_3)_4Si$, $CFCl_3$, and $XeOF_4$, respectively. The chemical shift convention used is that a positive (negative) sign indicates a chemical shift to high (low) frequency of the reference compound.

Raman Spectroscopy. The low-temperature Raman spectra of $[F_5SNH_3][AsF_6]$ (–160 °C) and $[F_5SN(H)Xe][AsF_6]$ (–45 °C) were recorded on a Bruker RFS 100 FT Raman spectrometer using 1064-nm excitation and a resolution of 1 cm^{-1}, as previously described.[51] The spectra were recorded using a laser power of 300 mW and a total of 600 and 10 000 scans, respectively, for acquisition of the spectra.

Computational Methods. Quantum-chemical calculations were carried out using MP2 and SVWN (DFT) methods and the program Gaussian 03[56] for geometry optimizations and vibrational frequencies and intensities for the $F_5SNH_3^+$ and $F_5SN(H)Xe^+$ cations, and the $[F_5SN(H)Xe][AsF_6]$ ion pair. The standard all-electron cc-pVTZ basis set, as implemented in the Gaussian program, was utilized for all elements except Xe and As, for which the semirelativistic large core pseudopotential basis set SDB-cc-pVTZ was used.[57] The combined use of cc-pVTZ and SDB-cc-pVTZ basis sets is indicated by (SDB-)cc-pVTZ. The program GaussView[58] was used to visualize the vibrational displacements that form the basis of the vibrational mode descriptions given in Tables 4, 5, and S3.

Acknowledgment. We thank the Natural Sciences and Engineering Research Council (NSERC) of Canada for financial support in the form of a research grant (G.J.S.); the Ontario Ministry of Training, Colleges and Universities and the McMaster University Centennial Scholarship Fund for the award of graduate scholarships (G.L.S.); Dr. J. C. P. Sanders and N. T. Arner for preliminary NMR work; and SHARCNet (Shared Hierarchical Academic Research Computing Network; www.sharcnet.ca) for computational resources.

(54) Sheldrick, G. M. *SADABS (Siemens Area Detector Absorption Corrections)*; University of Göttingen: Göttingen, Germany. Personal communication, 1998.

(55) *SHELXTL-Plus*, release 5.1; Siemens Analytical X-ray Instruments, Inc.: Madison, WI, 1998.

(56) Frisch, M. J.; Trucks, G. W.; Schlegel, H. B.; Scuseria, G. E.; Robb, M. A.; Cheeseman, J. R.; Zakrzewski, V. G.; Montgomery, J. A., Jr.; Stratmann, R. E.; Burant, J. C.; Dapprich, S.; Millam, J. M.; Daniels, A. D.; Kudin, K. N.; Strain, M. C.; Farkas, O.; Tomasi, J.; Barone, V.; Cossi, M.; Cammi, R.; Mennucci, B.; Pomelli, C.; Adamo, C.; Clifford, S.; Ochterski, J.; Petersson, G. A.; Ayala, P. Y.; Cui, Q.; Morokuma, K.; Salvador, P.; Dannenberg, J. J.; Malick, D. K.; Rabuck, A. D.; Raghavachari, K.; Foresman, J. B.; Cioslowski, J.; Ortiz, J. V.; Baboul, A. G.; Stefanov, B. B.; Liu, G.; Liashenko, A.; Piskorz, P.; Komaromi, I.; Gomperts, R.; Martin, R. L.; Fox, D. J.; Keith, T.; Al-Laham, M. A.; Peng, C. Y.; Nanayakkara, A.; Challacombe, M.; Gill, P. M. W.; Johnson, B.; Chen, W.; Wong, M. W.; Andres, J. L.; Gonzalez, C.; Head-Gordon, M.; Replogle, E. S.; Pople, J. A. *Gaussian 98*, revision A.11; Gaussian, Inc.: Pittsburgh, PA, 2003.

(57) Basis sets were obtained from the Extensible Computational Chemistry Environment Basis set Database, version 2/25/04, as developed and distributed by the Molecular Science Computing Facility, Environmental and Molecular Science Laboratory, which is part of the Pacific Northwest Laboratory, P.O. Box 999, Richland, WA 99352.

(58) *GaussView*, release 3.0; Gaussian Inc.: Pittsburgh, PA, 2003.

Supporting Information Available: Bond valencies for $[F_5SN(H)Xe][AsF_6]$ and $[F_5TeN(H)Xe][AsF_6]$ (Table S1); experimental and calculated bond lengths and angles for the $[F_5SN(H)Xe][AsF_6]$ ion pair (Table S2); experimental and calculated vibrational frequencies, intensities, and assignments for the $[F_5SN(H)Xe][AsF_6]$ ion pair (Table S3); experimental and calculated geometric parameters, vibrational frequencies, assignments, and calculated NBO data for SF_6 and F_5SCl (Table S4); factor-group analyses for $F_5SN(H)Xe^+$ and AsF_6^- in $[F_5SN(H)Xe][AsF_6]$ (Table S5); ^{19}F NMR spectrum of $[F_5SNH_3][AsF_6]$ (Figure S1); and an X-ray crystallographic file in CIF format for the structure determination of $[F_5SN(H)Xe][AsF_6]$. This material is available free of charge via the Internet at http://pubs.acs.org.

IC702039F